

See discussions, stats, and author profiles for this publication at: <https://www.researchgate.net/publication/272089721>

# Redox-active on-surface polymerization of single-site divalent cations from pure metals by a ketone-functionalized phenanthroline

ARTICLE *in* THE JOURNAL OF CHEMICAL PHYSICS · JANUARY 2015

Impact Factor: 2.95 · DOI: 10.1063/1.4906894

---

CITATIONS

2

READS

31

## 5 AUTHORS, INCLUDING:



Daniel Skomski

Indiana University Bloomington

7 PUBLICATIONS 36 CITATIONS

[SEE PROFILE](#)



Christopher Tempas

Indiana University Bloomington

4 PUBLICATIONS 12 CITATIONS

[SEE PROFILE](#)



Gregory S. Bukowski

Indiana University Bloomington

1 PUBLICATION 2 CITATIONS

[SEE PROFILE](#)



Steven L Tait

Indiana University Bloomington

43 PUBLICATIONS 1,064 CITATIONS

[SEE PROFILE](#)



## Redox-active on-surface polymerization of single-site divalent cations from pure metals by a ketone-functionalized phenanthroline

Daniel Skomski, Christopher D. Tempas, Gregory S. Bukowski, Kevin A. Smith, and Steven L. Tait

Citation: *The Journal of Chemical Physics* **142**, 101913 (2015); doi: 10.1063/1.4906894

View online: <http://dx.doi.org/10.1063/1.4906894>

View Table of Contents: <http://scitation.aip.org/content/aip/journal/jcp/142/10?ver=pdfcov>

Published by the AIP Publishing

---

### Articles you may be interested in

Ferroelectric like characteristics in redox active polymer of 5,10,15,20 tetra(4-hydroxyphenyl)-porphyrin at room temperature

*Appl. Phys. Lett.* **103**, 033302 (2013); 10.1063/1.4813736

Healing of oxygen vacancies on reduced surfaces of gold-doped ceria

*J. Chem. Phys.* **130**, 144702 (2009); 10.1063/1.3110702

Gas binding to Au 13 , Au 12 Pd , and Au 11 Pd 2 nanoclusters in the context of catalytic oxidation and reduction reactions

*J. Chem. Phys.* **129**, 164712 (2008); 10.1063/1.2993252

O 2 evolution on a clean partially reduced rutile TiO 2 ( 110 ) surface and on the same surface precovered with Au 1 and Au 2 : The importance of spin conservation

*J. Chem. Phys.* **129**, 074705 (2008); 10.1063/1.2956506

K and mixed K + O adlayers on Rh(110)

*J. Chem. Phys.* **124**, 014706 (2006); 10.1063/1.2140693

---

The banner features the AIP logo and the journal name. Below it, the text "Meet The New Deputy Editors" is displayed. Four circular portraits of the editors are shown, each with their name below it: Peter Hamm, David E. Manolopoulos, and James L. Skinner. The background is a dark blue with colorful, abstract, radiating patterns resembling fireworks or molecular structures.

# Redox-active on-surface polymerization of single-site divalent cations from pure metals by a ketone-functionalized phenanthroline

Daniel Skomski, Christopher D. Tempas, Gregory S. Bukowski, Kevin A. Smith,  
and Steven L. Tait<sup>a)</sup>

*Department of Chemistry, Indiana University, 800 E. Kirkwood Ave., Bloomington, Indiana 47405, USA*

(Received 21 November 2014; accepted 14 January 2015; published online 10 February 2015)

Metallic iron, chromium, or platinum mixing with a ketone-functionalized phenanthroline ligand on a single crystal gold surface demonstrates redox activity to a well-defined oxidation state and assembly into thermally stable, one dimensional, polymeric chains. The diverging ligand geometry incorporates redox-active sub-units and bi-dentate binding sites. The gold surface provides a stable adsorption environment and directs growth of the polymeric chains, but is inert with regard to the redox chemistry. These systems are characterized by scanning tunnelling microscopy, non-contact atomic force microscopy, and X-ray photoelectron spectroscopy under ultra-high vacuum conditions. The relative propensity of the metals to interact with the ketone group is examined, and it is found that Fe and Cr more readily complex the ligand than Pt. The formation and stabilization of well-defined transition metal single-sites at surfaces may open new routes to achieve higher selectivity in heterogeneous catalysts. © 2015 AIP Publishing LLC. [<http://dx.doi.org/10.1063/1.4906894>]

## I. INTRODUCTION

To achieve high levels of selectivity in next-generation catalysts and more fully understand their active sites, metal sites of a well-defined chemical state and highly regular structure must be stabilized on surfaces. Here, we report the formation of single-site  $M^{2+}$  centers within phenanthroline-coordinated polymers, which are generated directly from metallic iron, chromium, and platinum on the Au(100) surface. Effective molecular design, incorporating redox-active sub-units with bi-dentate binding pockets in a diverging structural geometry, realizes both redox activity and molecular self-assembly of single-site metal centers into thermally stable metal-ligand polymers.

Platinum has important applications in catalysis for carbophilic activation,<sup>1–3</sup> oxygen reduction,<sup>4</sup> and other reactions in solution-phase systems and was previously studied by our research group in on-surface organization with a tetrazine-based ligand.<sup>5</sup> However, such a ligand-based redox strategy had not been applied to more earth abundant metals, such as iron and chromium, utilizing common and readily available ligands, such as phenanthroline. Chromium is widely used as a catalyst in the industrial-scale production of polyethylene<sup>6</sup> and for oxidation reactions,<sup>7</sup> but it had not previously been studied in the on-surface assembly of metal coordination networks. Iron is a catalyst in hydrocarbon,<sup>8</sup> ammonia,<sup>9</sup> and chiral product formation<sup>10</sup> and has been studied in surface assembly with carboxylic acid and pyridyl functionalized ligands.<sup>11–14</sup>

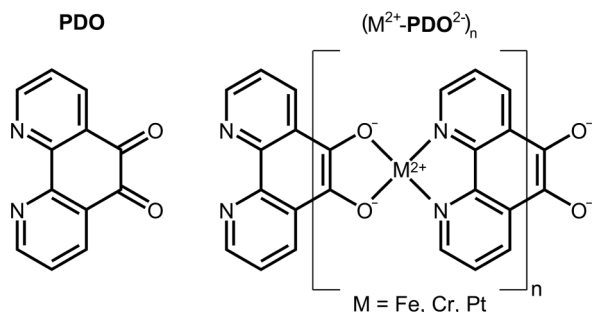
A common challenge with the use of each of these metals in traditional heterogeneous catalyst design is the tendency to form nanoparticles, which have a variety of local atomic coordination environments. It is for this reason that heterogeneous

catalysts generally suffer from poor selectivity compared to the well-defined inorganic metal-ligand complexes typical of homogenous catalysts. A central goal of this study is to develop surface-supported transition metal centers with a well-defined oxidation state and a high degree of uniformity across the surface. This could potentially lead to surface catalysts with chemically uniform reaction sites.

Phenanthrolines are among the best coordinating agents<sup>15</sup> and have important applications in catalysis, e.g., for oxidation of alcohols,<sup>16</sup> benzene arylation,<sup>17</sup> and copolymerization.<sup>18</sup> In addition, they are also used for ion transport and as ion-selective sensors.<sup>19</sup> While phenanthrolines have been used extensively in solution chemistry, only a few surface studies had been conducted<sup>20–22</sup> and the capability of the ligands to achieve on-surface redox reactions to produce a divalent metal chemical state and assembly into metal-ligand polymers had not been realized. In this study, a diketone-functionalized phenanthroline (1,10-phenanthroline-5,6-dione, **PDO**, Scheme 1) was chosen as ligand for two key properties. First, the oxidative potential for stabilizing metal dication in two bidentate sites is desirable here to produce a well-defined oxidation state of the coordinated metal centers. Second, the diverging ligand geometry can lead to extended polymeric chains on the surface, thus producing highly uniform coordination environments for the metal centers and also contributing to the excellent thermal stability of the systems. The diverging geometry of a single ligand also allows for a higher surface concentration of single-site metal centers than could be achieved with a bulkier multi-ligand complex or porphyrin-type complexation.

In this work, we demonstrate that sequential deposition of **PDO** and any one of the three metals studied (Fe, Cr, or Pt) leads to an on-surface redox reaction producing 1D polymer chains of oxidized metal sites and reduced ligands. X-ray photoelectron spectroscopy (XPS) provides clear

<sup>a)</sup>tait@indiana.edu

SCHEME 1. PDO ligand used in this study and the  $(M^{2+}\text{-PDO}^{2-})_n$  polymer.

evidence for the on-surface redox chemistry. Molecular-resolution scanning tunnelling microscopy (STM) and non-contact atomic force microscopy (NC-AFM) allow detailed structural characterization. Finally, experiments conducted at elevated temperatures demonstrate excellent thermal stability of the polymeric chains.

## II. MATERIALS AND METHODS

The experiments were conducted in a pristine ultra-high vacuum (UHV) system ( $<5 \times 10^{-10}$  Torr). The reconstructed gold (100) single crystal was cleaned by numerous cycles of argon ion sputtering (with the sample held at 200 °C) and thermal annealing to 500 °C. Under these conditions, the Au(100) surface spontaneously reconstructs to a quasi-hexagonal (26×68) reconstruction.<sup>23,24</sup> The ligands 1,10-phenanthroline-5,6-dione (PDO, 97%, Sigma-Aldrich), platinum-octaethylporphyrin (Pt-OEP, 98%, Sigma-Aldrich), and octaethylporphyrine (OEP, Frontier Scientific, >95%) were deposited from a Knudsen-type evaporator in UHV at sublimation temperatures of 100 °C, 210 °C, and 210 °C, respectively, after degassing for many hours in UHV. Platinum (99.95% pure rod, Goodfellow), iron (99.95% pure rod, Goodfellow), and chromium (99.995% pure chips, Sigma-Aldrich) were vapor deposited using an electron beam evaporator (QUAD-EV-S Mini e-beam Evaporator, Mantis Deposition, Ltd.).

The system is equipped with both STM and NC-AFM (SPM UHV 750, RHK Technologies) as well as XPS (electron energy analyzer PHOIBOS 150 and Mg/Al dual anode X-ray source XR-50, SPECS GmbH). STM imaging and XPS acquisition were conducted at room temperature and at elevated temperatures. The well-characterized (3×3) structure of terephthalic acid on the copper (100) surface<sup>11,25,26</sup> was used to calibrate the STM/NC-AFM instrument. Sharp tungsten STM tips were fabricated by electrochemical etching. Bias voltages of 1.0–1.2 V and set point currents from 0.2 to 0.4 nA were generally used for the STM imaging. The AFM was operated in non-contact mode with antimony-doped single crystal silicon cantilevers (NSG10, NT-MDT Co.,  $f_0 = 280$  kHz) and frequency shift setpoints of 18–20 Hz. STM/NC-AFM image analysis was conducted using the WSxM software.<sup>27</sup> The interconnected vacuum chambers allow for sample cleaning, vapour deposition, STM/NC-AFM, and XPS on the same samples without removal from the UHV environment.

## III. RESULTS AND DISCUSSION

### A. On-surface redox chemistry

STM observations show formation of 1D polymeric chains upon co-deposition of metals and ligands (Figure 1). The redox chemistry of the metal-ligand bonding in these chains is studied here by XPS. Measurements of the Fe 2p, Cr 2p, and Pt 4f photoelectron peaks clearly indicate oxidation of the metals to the +2 charge state upon addition of PDO. In each case, this is evident as a 2 eV chemical shift to higher binding energy, as shown in Figure 2 (note that the binding energy scale on the horizontal axis is different in each panel due to the difference in the spin-orbital splitting for each metal; spectra showing the data with the same binding energy scale are provided in Figure S1<sup>29</sup>). These peaks for these different metals are known from prior studies to each have a different width.<sup>28</sup> A complete list of XPS peak positions from this study and comparison to relevant reference literature are provided in the supplementary material.<sup>29</sup>

The XPS binding energy (BE) values are Fe 2p<sub>3/2</sub> 710.4 eV (Fe-PDO), Cr 2p<sub>3/2</sub> 575.9 eV (Cr-PDO), and

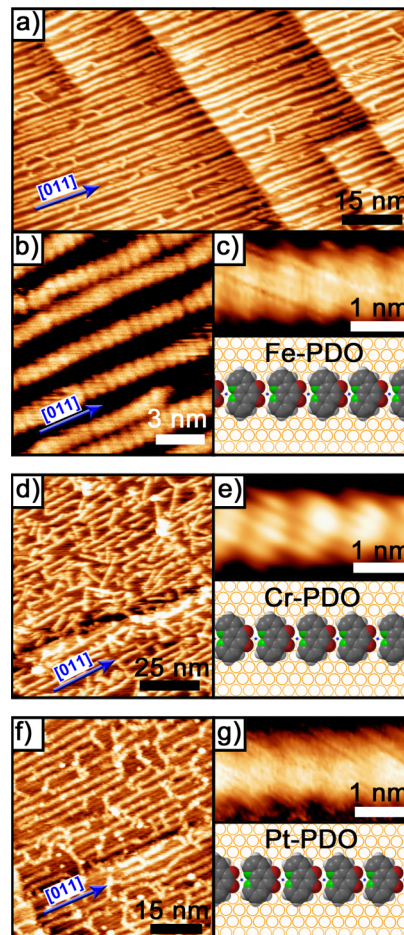


FIG. 1. Room-temperature STM images of PDO with Fe, Cr, or Pt on the reconstructed Au(100) surface after annealing at 100 °C for 10 min. Images of metal-ligand chains are shown for ((a)–(c)) Fe-PDO, ((d) and (e)) Cr-PDO, and ((f) and (g)) Pt-PDO, including ((a), (b), (d), and (f)) wide scan views of chains and ((c), (e), and (g)) close-up images with corresponding models to resolve chain structure. Note that each of the close-up images and models is presented at the same scale (overlay versions of the close-up images with models are presented in Fig. S5<sup>29</sup>).

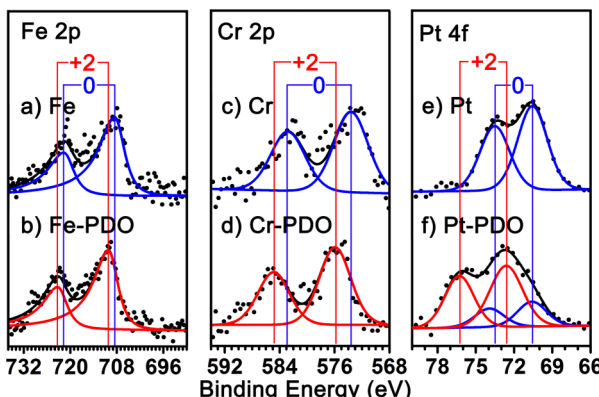


FIG. 2. ((a) and (b)) Iron 2*p*, ((c) and (d)) chromium 2*p*, and ((e) and (f)) platinum 4*f* XPS photoelectron peaks ((a), (c), and (e)) in their pure metallic (charge neutral) form and ((b), (d), (f)) after complexation with **PDO** on the reconstructed Au(100) surface. Spectra were acquired at room temperature after annealing at 100–120 °C for 10 min. The oxidation of the metals by **PDO** is evidenced by 2 eV chemical shifts to higher BE (note that BE scale is different in each panel, see Figure S1<sup>29</sup>). See supplementary material for a complete list of XPS peak positions from this study and comparison to reference literature.<sup>29</sup>

**Pt 4*f*<sub>7/2</sub> 72.6 eV (Pt-PDO).** The Fe 2*p* BE of Fe(II)-ligand species on the reconstructed Au(100) surface was not previously reported, but the chemical shift in the conversion of metallic Fe to Fe-PDO in this work (1.9 eV) matches the difference in BE between bulk metallic Fe and bulk Fe(II)-phthalocyanine (2.1 eV).<sup>28</sup> The Pt and Cr measurements are in agreement with Pt(II)-3,6-di-2-pyridyl-1,2,4,5-tetrazine and Cr(II)-octaethylporphyrin, respectively, for which we acquired data on the same reconstructed Au(100) surface (see supplementary material<sup>29</sup>). When **PDO** is deposited to Fe and Cr, the photoelectron peak widths remain the same, but the positions shift. (Note that all peak positions are measured relative to the position of the Au 4*f* peak.) In each spectrum, a fit is made by allowing two sets of peak components based on reference values for (1) metal and (2) +2 oxidation state (Figure 2). Each of these sets contains two peaks due to spin-orbit coupling, which are locked at exact peak separation,  $\Delta BE$ , and area ratios as discussed in Section S1 of the supplementary material.<sup>29</sup> In the case of Fe-PDO and Cr-PDO, the data are fit well by the oxidized component set only. With Pt, on the other hand, the peak width in Figure 2(f) is noticeably larger than in Figure 2(e) (3.5 eV vs. 2.5 eV FWHM); therefore, an additional pair of components is added to fit the data, corresponding to metallic Pt. Note that this is consistent with the STM observation (Figure 1) that Fe-PDO and Cr-PDO chains are better ordered than Pt-PDO, indicating that the Fe and Cr more readily complex **PDO** than does Pt.

XPS measurements of the O 1*s* and N 1*s* photoelectron peaks also indicate coordinative bonding. **PDO** exhibits an O 1*s* chemical shift to lower BE upon metal complexation (Figures 3(a) and 3(b)). The chemical shift is expected for coordinative reduction of oxygen<sup>25</sup> yielding metal-alkoxide. **PDO** also exhibits a chemical shift in the N 1*s* photoelectron peak to higher BE (Figures 3(c) and 3(d)). The chemical shift is consistent with the coordination of pyridyl-like nitrogen atoms to a transition metal di-cation;<sup>5,30,31</sup> i.e., the N1s electrons are

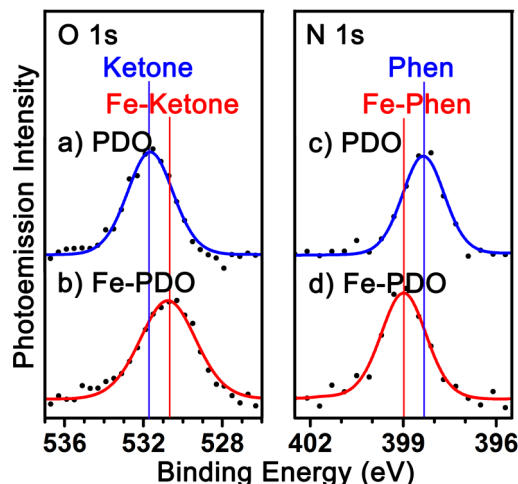


FIG. 3. ((a) and (b)) Oxygen 1*s* and ((c) and (d)) nitrogen 1*s* XP spectra of ((a) and (c)) **PDO** and ((b) and (d)) **Fe-PDO** on the reconstructed Au(100) surface acquired at room temperature after annealing at 100 °C for 10 min. Peak positions for these data are listed in Table S6 and corresponding data for Pt-PDO and Cr-PDO are listed in Tables S5 and S7, respectively.<sup>29</sup>

more tightly bonded in this environment due to lone pair interaction with M<sup>2+</sup> acting as a Lewis acid.

**PDO** reduction is further confirmed by a comparison of C 1*s* XPS spectra before and after Fe addition. The C 1*s* signal of pure **PDO** (Figure 4(a)) shows two components in the expected 1:5 ratio (1 ketone C:5 phenanthroline C). After Fe addition and annealing, only one C 1*s* feature is observed (Figure 4(d)) with no change in the overall C 1*s* peak area, consistent with the involvement of the ketone in the redox polymerization causing a shift to lower BE. A chemical shift to lower BE in the C 1*s* ketone signal has been observed in analogous systems, e.g., reduction of carboxylic acid to carboxylate.<sup>25</sup> A similar chemical shift is also observed for the Cr and Pt system (see supplementary material<sup>29</sup>).

These XPS results confirm the oxidative potential of the diketone-functionalized phenanthroline for stabilizing metal

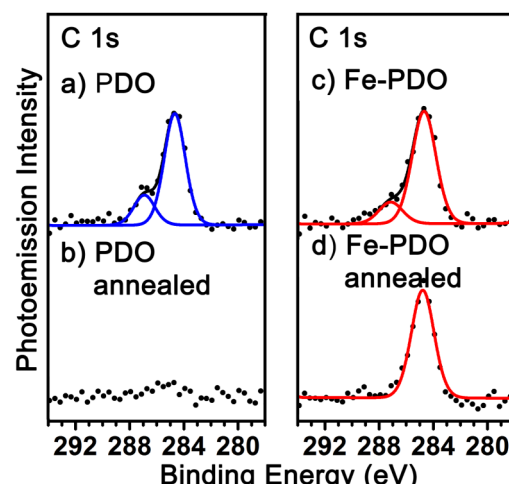


FIG. 4. Carbon 1*s* XP spectra of ((a) and (b)) **PDO** and ((c) and (d)) **Fe-PDO** on the reconstructed Au(100) surface acquired at room temperature ((a) and (c)) before and ((b) and (d)) after annealing at 200 °C for 10 min. The loss of signal in (b) indicates desorption of the uncomplexed **PDO** at this temperature.

dications on the Au(100) surface. This redox process does not require diatomic elimination as has been observed in on-surface complexation of metals with different classes of ligands, such as porphyrins<sup>32,33</sup> and carboxylic acids<sup>12</sup> on less inert metal surfaces (metal surface catalysed processes). In future studies, the wide range of design parameters available in on-surface redox formation of metal-ligand polymer systems, like the system studied here, could potentially achieve metal oxidation states that have not yet been accessed in the vapor deposition of pre-formed metal-ligand complexes to surfaces.

## B. Metal-ligand polymer chain structure

High-resolution STM images indicate the formation of 1D metal-ligand polymers of the form  $(\text{PDO}^{2-}\text{-M}^{2+})_n$ . The chains form by coordination of the metal at the N and O sites (see the models in Figure 1). The **M-PDO** chains are oriented parallel to the Au reconstruction rows, regardless of the choice of metal or order of deposition (Figure 5). The appearance and spacing of features along the chains are uniform in the STM measurements, which is consistent with all of the molecules in a given chain assuming the same orientation; i.e., each single metal ion is bound on one side by a bidentate N from the phenanthroline and on the other side by a bidentate O from diketone. Such a configuration avoids the H steric clash which would occur if the molecules had an alternatingly anti-parallel orientation along the chain to form a binding pocket of either all N or all O.<sup>34</sup> The intermolecular spacing of  $8.3 \pm 0.4 \text{ \AA}$  is identical with the different metals, likely due to the similarity in ionic radii ( $0.63 \text{ \AA}$ ,  $0.73 \text{ \AA}$ , and  $0.60 \text{ \AA}$  in 4-coordinate crystal structures of  $\text{Fe}^{2+}$ ,  $\text{Cr}^{2+}$ , and  $\text{Pt}^{2+}$ , respectively<sup>35</sup>), registry with the Au surface atomic spacing ( $3 \times 2.76 \text{ \AA} = 8.28 \text{ \AA}$ <sup>36–38</sup>), and some relaxation of the quasi-square planar coordination geometry. The M–N and M–O bond lengths in this structure are about  $2.0\text{--}2.5 \text{ \AA}$ , which are consistent with expected bond lengths in solution-phase inorganic complexes.<sup>39,40</sup>

The structure and bonding geometries of the metals on the surface differ from solution phase systems,<sup>41</sup> where structures with coordination numbers greater than four are common, suggesting the importance of the substrate in guiding the assembly of species which would otherwise partake in a

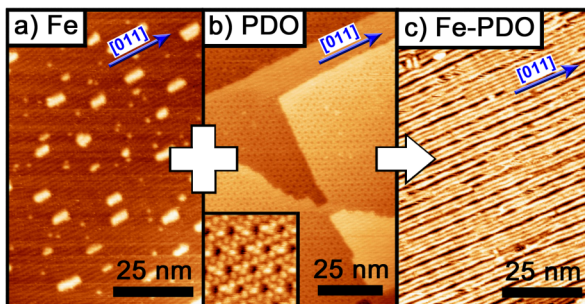


FIG. 5. Room-temperature STM images of Fe, **PDO**, and **Fe-PDO** on the reconstructed Au(100) surface. (a) Nanometer-scale 2D Fe islands. (b) Packing structure of pure **PDO** with inset image of dimensions  $8 \text{ nm} \times 8 \text{ nm}$ . (c) Surface in (a), after addition of **PDO** and annealing at  $125^\circ\text{C}$  for 10 min. Note that adding ligand to pre-deposited metal (c) produces the same 1D polymer structure as adding metal to pre-deposited ligand (Figures 1(a)–1(c)), i.e., final structure is independent of deposition order.

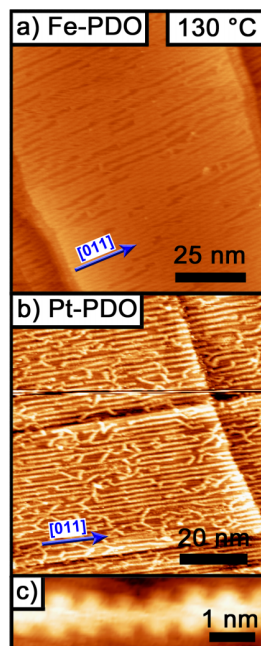


FIG. 6. STM images of intact  $(\text{PDO}^{2-}\text{-M}^{2+})_n$  chains on the reconstructed Au(100) surface, during and after thermal annealing. (a) High-temperature STM image of Fe-**PDO** chains acquired at a sample temperature of  $130^\circ\text{C}$ . (b) Room-temperature STM image of Pt-**PDO** chains after annealing at  $250^\circ\text{C}$  for 15 min. (c) Room-temperature STM zoom-in image of one chain of Pt-**PDO** after annealing at  $300^\circ\text{C}$  for 10 min.

diversity of bonding geometries. The metal cations are not clearly visualized in many of the STM images; this effect has also been observed with other transition metal cations<sup>42</sup> and is likely due to a mismatch in the electronic density of states and the small size of the di-cations. However, in a few STM images, the metal centers are clearly visualized (Figure 6(c)). NC-AFM images of the 1D **M-PDO** chain structure are consistent with the STM data (Figure S4<sup>29</sup>).

The metal-ligand structures differ from the structures observed for assembly of either the metal alone or the **PDO** ligand alone. The pure metal (Figure 5(a)) and pure **PDO** (Figure 5(b)) form 2D phases on the Au surface, which are clearly distinct from the 1D chains of the mixed structure. We note that the rows of the  $c(26 \times 68)$  reconstruction of the Au(100) surface<sup>23,24</sup> are observed in the STM images. When Fe is deposited without ligand on the reconstructed Au(100) surface, 2D metal islands grow anisotropically with elongation along the direction of the gold reconstruction.<sup>43</sup> Anisotropic 2D islands are also formed with Pt and Cr. In the case of the pure **PDO** structure (Figure 5(b)), note that the total coverage on the surface was less than one monolayer); a porous 2D framework is formed. This framework is likely stabilized by intermolecular hydrogen bonds.

The formation of the 1D polymers is independent of the ligand and metal deposition order. While most experiments were performed by reacting the pure **PDO** structure with subsequent addition of metal (as in Figure 1), the pure metal 2D islands are dissolved with addition of **PDO** and result in the same 1D chains. For example, the same sample that was initially composed only of Fe islands on Au (Figure 5(a)) is transformed into a highly ordered set of 1D Fe-**PDO** chains upon **PDO** deposition and annealing (Figure 5(c)).

The same result is also observed with Pt (Figure S2<sup>29</sup>). This dissolution of the metal islands suggests strong interactions with the ligand and has been reported previously, e.g., with Co metal and terephthalate ligands<sup>44</sup> and for Pt with tetrazine ligands.<sup>5</sup>

Fe and Cr more readily form complexes with **PDO** than Pt. In the STM data, after annealing at 100 °C for 10 min, the **Pt-PDO** surface is composed of 1D chains along with small 2D metal islands. The STM images are consistent with the XPS data, indicating primarily oxidized Pt but also a minority of metallic Pt species. This poor complexation of Pt is in contrast to the very efficient complexation of Fe and Cr by **PDO** observed here (XPS shows virtually no charge-neutral metal, Fig. 2) and to the previously reported complexation of Pt with tetrazine ligands.<sup>5</sup>

We also note in the case of **Pt-PDO** and **Cr-PDO** that there is a higher occurrence of structural irregularities, such as non-linear (curved) polymer chains and junctions between chains at different angles. It is possible that the poor complexation of Pt by **PDO** may be partially responsible for these effects, as sites rich in Pt metal (appearing as bright dots in the STM data, e.g., Fig. 1(f)) are sites where chains may grow into each other at various angles. In the case of **Cr-PDO** (Fig. 1(d)), we observe some polymers in directions that are not parallel to the Au reconstruction and some curved chains, despite the fact that XPS indicates effective complexation of Cr. It is possible that this may be due to the ability of Cr<sup>2+</sup> to accommodate a variety of bonding geometries,<sup>45</sup> i.e., that the coordination at the cross-linked sites may not be square planar. The relative propensity of certain metals to complex with different organic functional groups in surface-supported systems<sup>46</sup> is a subject of on-going studies.

### C. Thermal stability

The resulting **M-PDO** polymers afford high thermal stability. While the pure ligand thermally desorbs from Au(100) at 200 °C (Figures 4(a) and 4(b)), it is stabilized against desorption in the metal-ligand chain complex (Figures 4(c) and 4(d)). High-temperature XPS measurements of all three metal-ligand structures were conducted while each sample was held at 200 °C (Figures 7(a), 7(c), and 7(e)) and show that the metal oxidation state is unchanged at this elevated temperature, i.e., the 1D polymer chains remain intact. XPS measurements were also taken at room temperature after annealing at 300 °C (Figures 7(b), 7(d), and 7(f)) and also show that the metal oxidation state has remained unchanged at 300 °C. This indicates that the chains remain intact at 300 °C because if they had decomposed into free ligands and metal atoms, the ligands would have desorbed from the surface at this temperature (see Figure 4(b), which shows evidence of uncomplexed ligand desorption at 200 °C). The spectra corresponding to the **M-PDO** structures of all three metals after high temperature annealing remain unchanged compared to mild annealing conditions (Figure 2), i.e., the redox state of Fe<sup>2+</sup>, Cr<sup>2+</sup>, and Pt<sup>2+</sup> is maintained during and after thermal annealing.

High-temperature STM experiments were conducted of **Fe-PDO** at 130 °C and show that the 1D polymers remain

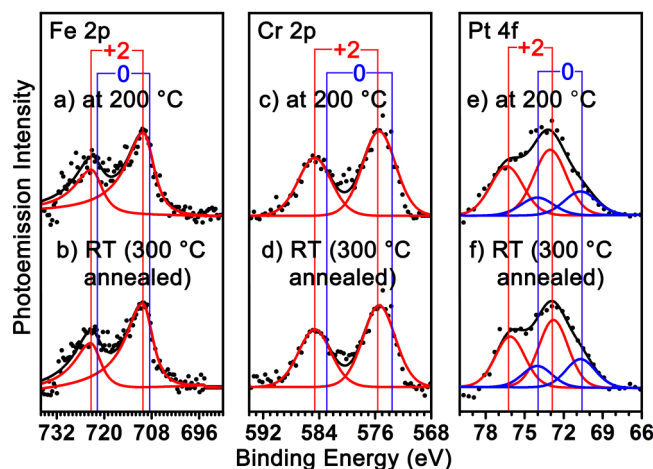


FIG. 7. ((a) and (b)) Iron 2p, ((c) and (d)) chromium 2p, and ((e) and (f)) platinum 4f XPS photoelectron peaks demonstrating the thermal stability of **M-PDO** bonding in 1D polymeric chains on Au(100). ((a), (c), and (e)) XP spectra acquired with the sample temperature held at 200 °C after annealing at 250 °C for 10 min. ((b), (d), and (e)) XP spectra obtained at room temperature on the same samples as in ((a), (c), and (e)) after further annealing at 300 °C for 10 min.

intact at elevated temperatures, demonstrating excellent thermal stability locally (Figure 6(a)). STM measurements of the **Pt-PDO** structure at room temperature after annealing at 250–300 °C (Figures 6(b) and 6(c)) show that the 1D polymers remain ordered. Atomic-resolution STM images of the chains (Figure 6(c)), which resolve both the ligand and metal ions, confirm that the high annealing temperatures did not alter the chain structure. The thermal stability of these systems is promising for potential application in heterogeneous catalysis.

### IV. CONCLUSIONS

The functionalization of the phenanthroline core, as demonstrated here with ketone, highlights the capability of the ligand to achieve redox activity during assembly into metal-ligand polymers. The redox-active ketone units and bi-dentate binding pockets arranged in a diverging structural geometry allow formation of single-site metal centers with a well-defined chemical and structural state, utilizing platinum as well as earth-abundant metals iron and chromium. While all three metals form the same polymer chain structure, Fe and Cr more readily complex the ligand as compared to Pt, which raises interesting questions about the relative propensity of certain metals to interact with the ketone group. The thermally stable metal-phenanthrolines serve as easily tuned model systems for single-site metal centers at surfaces that could be developed into support structures for future applications in catalysis. Future experiments are planned to study an increasing variety of ligands to better understand the effects of ligand binding pockets and metal coordination geometries.

### ACKNOWLEDGMENTS

This work was supported by the Chemical Sciences, Geosciences, and Biosciences Division, Office of Basic Energy Sciences, Office of Science, U.S. Department of Energy, Grant No. DE-FG02-12ER16351.

- <sup>1</sup>R. A. Periana, D. J. Taube, S. Gamble, H. Taube, T. Satoh, and H. Fujii, *Science* **280**, 560 (1998).
- <sup>2</sup>M. Lersch and M. Tilset, *Chem. Rev.* **105**, 2471 (2005).
- <sup>3</sup>A. Fürstner and P. W. Davies, *Angew. Chem., Int. Ed.* **46**, 3410 (2007).
- <sup>4</sup>C. C. Liang and A. L. Juliard, *Nature* **207**, 629 (1965).
- <sup>5</sup>D. Skomski, C. D. Tempas, K. A. Smith, and S. L. Tait, *J. Am. Chem. Soc.* **136**, 9862 (2014).
- <sup>6</sup>M. P. McDaniel, *Adv. Catal.* **53**, 123 (2010).
- <sup>7</sup>J. Muzart, *Chem. Rev.* **92**, 113 (1992).
- <sup>8</sup>C. Bolm, J. Legros, J. Le Pailh, and L. Zani, *Chem. Rev.* **104**, 6217 (2004).
- <sup>9</sup>T. Kandemir, M. E. Schuster, A. Senyshyn, M. Behrens, and R. Schlögl, *Angew. Chem., Int. Ed.* **52**, 12723 (2013).
- <sup>10</sup>K. Gopalaiyah, *Chem. Rev.* **113**, 3248 (2013).
- <sup>11</sup>S. L. Tait, Y. Wang, G. Costantini, N. Lin, A. Baraldi, F. Esch, L. Petaccia, S. Lizzit, and K. Kern, *J. Am. Chem. Soc.* **130**, 2108 (2008).
- <sup>12</sup>M. A. Lingenfelder, H. Spillmann, A. Dmitriev, S. Stepanow, N. Lin, J. V. Barth, and K. Kern, *Chem. - Eur. J.* **10**, 1913 (2004).
- <sup>13</sup>A. Langner, S. L. Tait, N. Lin, C. Rajadurai, M. Ruben, and K. Kern, *Proc. Natl. Acad. Sci. U. S. A.* **104**, 17927 (2007).
- <sup>14</sup>S. Fabris, S. Stepanow, N. Lin, P. Gambardella, A. Dmitriev, J. Honolka, S. Baroni, and K. Kern, *Nano Lett.* **11**, 5414 (2011).
- <sup>15</sup>E. König, *Coord. Chem. Rev.* **3**, 471 (1968).
- <sup>16</sup>G. J. ten Brink, I. W. C. E. Arends, and R. A. Sheldon, *Science* **287**, 1636 (2000).
- <sup>17</sup>E. Shirakawa, K. Itoh, T. Higashino, and T. Hayashi, *J. Am. Chem. Soc.* **132**, 15537 (2010).
- <sup>18</sup>B. Milani, A. Anzilutti, L. Vicentini, A. S. O. Santi, E. Zangrando, S. Geremia, and G. Mestroni, *Organometallics* **16**, 5064 (1997).
- <sup>19</sup>J. A. McCleverty and T. J. Meyer, *Comprehensive Coordination Chemistry II: From Biology to Nanotechnology*, 1st ed. (Elsevier Pergamon, Amsterdam, 2004).
- <sup>20</sup>O. Domínguez, L. Echegoyen, F. Cunha, and N. J. Tao, *Langmuir* **14**, 821 (1998).
- <sup>21</sup>D. Payer, S. Rauschenbach, N. Malinowski, M. Konuma, C. Virojanadara, U. Starke, C. Dietrich-Buchecker, J. P. Collin, J. P. Sauvage, N. Lin, and K. Kern, *J. Am. Chem. Soc.* **129**, 15662 (2007).
- <sup>22</sup>A. M. Gao, X. R. Miao, J. Liu, P. Zhao, J. W. Huang, and W. L. Deng, *ChemPhysChem* **11**, 1951 (2010).
- <sup>23</sup>M. A. Vanhove, R. J. Koestner, P. C. Stair, J. P. Bibérian, L. L. Kesmodel, I. Bartoš, and G. A. Somorjai, *Surf. Sci.* **103**, 189 (1981).
- <sup>24</sup>M. A. Vanhove, R. J. Koestner, P. C. Stair, J. P. Bibérian, L. L. Kesmodel, I. Bartoš, and G. A. Somorjai, *Surf. Sci.* **103**, 218 (1981).
- <sup>25</sup>S. Stepanow, T. Strunkus, M. Lingenfelder, A. Dmitriev, H. Spillmann, N. Lin, J. V. Barth, C. Wöll, and K. Kern, *J. Phys. Chem. B* **108**, 19392 (2004).
- <sup>26</sup>Y. Ge, H. Adler, A. Theertham, L. L. Kesmodel, and S. L. Tait, *Langmuir* **26**, 16325 (2010).
- <sup>27</sup>I. Horcas, R. Fernández, J. M. Gómez-Rodríguez, J. Colchero, J. Gómez-Herrero, and A. M. Baro, *Rev. Sci. Instrum.* **78**, 013705 (2007).
- <sup>28</sup>J. F. Moulder and J. Chastain, *Handbook of X-ray Photoelectron Spectroscopy: A Reference Book of Standard Spectra for Identification and Interpretation of XPS Data* (Physical Electronics Division, Perkin-Elmer Corp., Eden Prairie, MN, 1992).
- <sup>29</sup>See supplementary material at <http://dx.doi.org/10.1063/1.4906894> for discussion of XPS analysis, comparison of XPS data, and additional STM and NC-AFM data.
- <sup>30</sup>S. Y. Gao, Y. B. Huang, M. N. Cao, T. F. Liu, and R. Cao, *J. Mater. Chem.* **21**, 16467 (2011).
- <sup>31</sup>J. Poppenberg, S. Richter, E. Darlatt, C. H. H. Traulsen, H. Min, W. E. S. Unger, and C. A. Schalley, *Surf. Sci.* **606**, 367 (2012).
- <sup>32</sup>Y. Bai, F. Buchner, M. T. Wendahl, I. Kellner, A. Bayer, H.-P. Steinrück, H. Marbach, and J. M. Gottfried, *J. Phys. Chem. C* **112**, 6087 (2008).
- <sup>33</sup>J. M. Gottfried, K. Flechtner, A. Kretschmann, T. Lukasczyk, and H. P. Steinrück, *J. Am. Chem. Soc.* **128**, 5644 (2006).
- <sup>34</sup>G. Wilkinson, R. D. Gillard, and J. A. McCleverty, *Comprehensive Coordination Chemistry: The Synthesis, Reactions, Properties & Applications of Coordination Compounds*, 1st ed. (Pergamon Press, Oxford, England, 1987).
- <sup>35</sup>D. R. Lide, *CRC Handbook of Chemistry and Physics*, 88th ed. (CRC Press, Boca Raton, FL, 2007).
- <sup>36</sup>Note: This value of Au nearest neighbor distance accounts for the reported 3.82% contraction in the surface layer upon reconstruction, as reported in the references cited here.
- <sup>37</sup>G. K. Binnig, H. Rohrer, C. Gerber, and E. Stoll, *Surf. Sci.* **144**, 321 (1984).
- <sup>38</sup>T. Schilling, B. Tesche, and G. Lehmpfuhl, *Z. Naturforsch. A* **47a**, 1187 (1992); PDF available at [http://zfn.mpdl.mpg.de/data/Reihe\\_A/47/ZNA-1992-47a-1187.pdf](http://zfn.mpdl.mpg.de/data/Reihe_A/47/ZNA-1992-47a-1187.pdf).
- <sup>39</sup>P. G. Rasmussen, J. E. Anderson, and J. C. Bayón, *Inorg. Chim. Acta* **87**, 159 (1984).
- <sup>40</sup>P. Kircher, G. Huttner, K. Heinze, B. Schiemenz, L. Zsolnai, M. Büchner, and A. Driess, *Eur. J. Inorg. Chem.* **1998**, 703.
- <sup>41</sup>E. D. Mckenzie, *Coord. Chem. Rev.* **6**, 187 (1971).
- <sup>42</sup>T. Ohshiro, T. Ito, P. Bühlmann, and Y. Umezawa, *Anal. Chem.* **73**, 878 (2001).
- <sup>43</sup>O. S. Hernán, A.L.V.de. Parga, J. M. Gallego, and R. Miranda, *Surf. Sci.* **415**, 106 (1998).
- <sup>44</sup>S. Clair, S. Pons, S. Fabris, S. Baroni, H. Brune, K. Kern, and J. V. Barth, *J. Phys. Chem. B* **110**, 5627 (2006).
- <sup>45</sup>K. H. Theopold, in *Encyclopedia of Inorganic Chemistry* (John Wiley & Sons, Ltd., 2006).
- <sup>46</sup>A. Langner, S. L. Tait, N. A. Lin, R. Chandrasekar, V. Meded, K. Fink, M. Ruben, and K. Kern, *Angew. Chem., Int. Ed.* **51**, 4327 (2012).